

Semi-automated software for the three-dimensional delineation of complex vascular networks

P. R. BARBER, B. VOJNOVIC, S. M. AMEER-BEG,
R. J. HODGKISS, G. M. TOZER & J. WILSON

Gray Cancer Institute, Mount Vernon Hospital, Northwood, Middlesex HA6 2JR, U.K.

Key words. Hough transform, image processing, image segmentation, *in vivo* microscopy, multi-photon microscopy, vascular network, window chamber model.

Summary

The understanding of tumour angiogenesis is of great importance in cancer research, as is the tumour response to vascular-targeted drugs. This paper presents software aimed at aiding these investigations and other situations where linear or dendritic structures are to be delineated from three-dimensional (3D) data sets. This software application was written to analyse the data from 3D data sets by allowing the manual and semi-automated tracking and delineation of the vascular tree, including the measurement of vessel diameter. A new algorithm, CHARM, based on a compact Hough transform and the formation of a radial map, has been used to locate vessel centres and measure diameters automatically. The robustness of this algorithm to image smoothing and noise has been investigated.

Introduction

In cancer research, the study of the structure of vascular networks *in vivo* is crucial to the understanding of tumour angiogenesis and the response to vascular-targeted drugs. There is currently much interest in examining the methods of action of drugs, such as combretastatin A4 phosphate, which have been shown to have an anticancer effect. This can be achieved through studies at the biochemical, cellular and complete tissue levels. This paper presents software aimed at aiding in investigations of the vascular structure of complete and living tissue and that may also be applicable to other problems in which similar structures are to be delineated from three-dimensional (3D) data sets.

In understanding the action of vasoactive drugs there is a need to measure, quantify and model vascular structures. Recent technological developments in two-photon fluorescence

microscopy have enabled the imaging, in three dimensions, of both normal and cancerous tissue within the dorsal skin flap of a rodent with the so-called 'window-chamber' (Tozer *et al.*, 2001). We have captured *in vivo* 3D data sets via a window-chamber arrangement with a multiphoton microscope (Ameer-Beg *et al.*, 2002) in a manner similar to that employed by Jain and co-workers (Brown *et al.*, 2001). In short, imaging contrast was achieved by intravenous injection of cascade-blue- or FITC-labelled high-molecular-weight (70-kDa) dextran, which acts as a fluorescent marker of blood plasma under two-photon excitation. This paper presents a software application that was written to analyse the data from such data sets by allowing the manual and semi-automated tracking and delineation of the vascular tree, including the measurement of vessel diameter. A particular problem is that the physical arrangement of the window chamber in the microscope limits the objective lenses that can be used to those of low magnification and low numerical aperture. The result is a highly nonspherically symmetric, optical point spread function (PSF).

There have previously been several approaches to the delineation of tree-like structures and there are commercial software applications available that can offer some automation in segmenting dendritic trees (e.g. 'NeuroneTracer', Bitplane, Zürich, Switzerland). Our images generally have highly complex and incomplete trees that may be disjointed, against a high-noise background and that are a challenge to segment by eye. The validation of any automated approach does require a gold standard, which at the present time is the manually segmented image. For this reason we thought it appropriate to form an application with a set of both manual and semi-automatic tracing tools.

Previously, other authors have targeted most efforts at producing algorithms for extracting information from 2D images and several of these were considered for a solution to the problem of automated tracing in three dimensions. Deformable models have been successful at solving medical image

segmentation problems (Bulpitt & Berry, 1998) similar to that presented here and are highly suited to extracting shapes from noisy data. These were considered unsuitable for application here as the detailed shape of the vasculature in cross-section is beyond the imaging resolution in the perpendicular (z) plane and a simpler approach could be used. The use of fuzzy clustering of profiles in relatively clean fundus images has also been successful in vessel tracking and the detection of junctions and branches (Tolias & Panas, 1998). In addition to these complex algorithms, and in recognition that manual segmentation is extremely powerful, a fully 3D, virtual reality workstation for the interactive manual segmentation of volumetric data is also under development elsewhere (Serra *et al.*, 1997).

Overview of user controls and functions

This section provides an overview of the functionality of the software, which can be seen visually in Fig. 1. Specific detail on the algorithms and processes can be found in the following section.

The user can load image stacks in the form of uncompressed .AVI files or Bio-Rad microscope .PIC files (Bio-Rad Laboratories Inc., CA, U.S.A.) directly, which can then be explored using three orthogonal views (XY , XZ and YZ). These types of 3D image files comprise a 'stack' of 2D (XY) images recorded at regular intervals in depth (Z). The display greyscale look-up table can be modified allowing the displayed images to be normalized for maximum contrast without loss of information or to have a user-defined linear look-up table applied. The current 3D position of the cursor can be moved with the mouse by clicking on the images or by using the position controls X , Y and Z on the left-hand panel. The user can zoom into a small area of the image around the cursor.

Linear structures can be traced by placing the cursor on the structure in the 3D image space using the three image views, or with numeric (x , y , z) position controls, and marking trace points. This process is eased with the z -plane auto-track function, which allows the user simply to specify the XY position on the XY image view and to have the cursor snap onto the nearest point of highest intensity in the Z direction. In this way

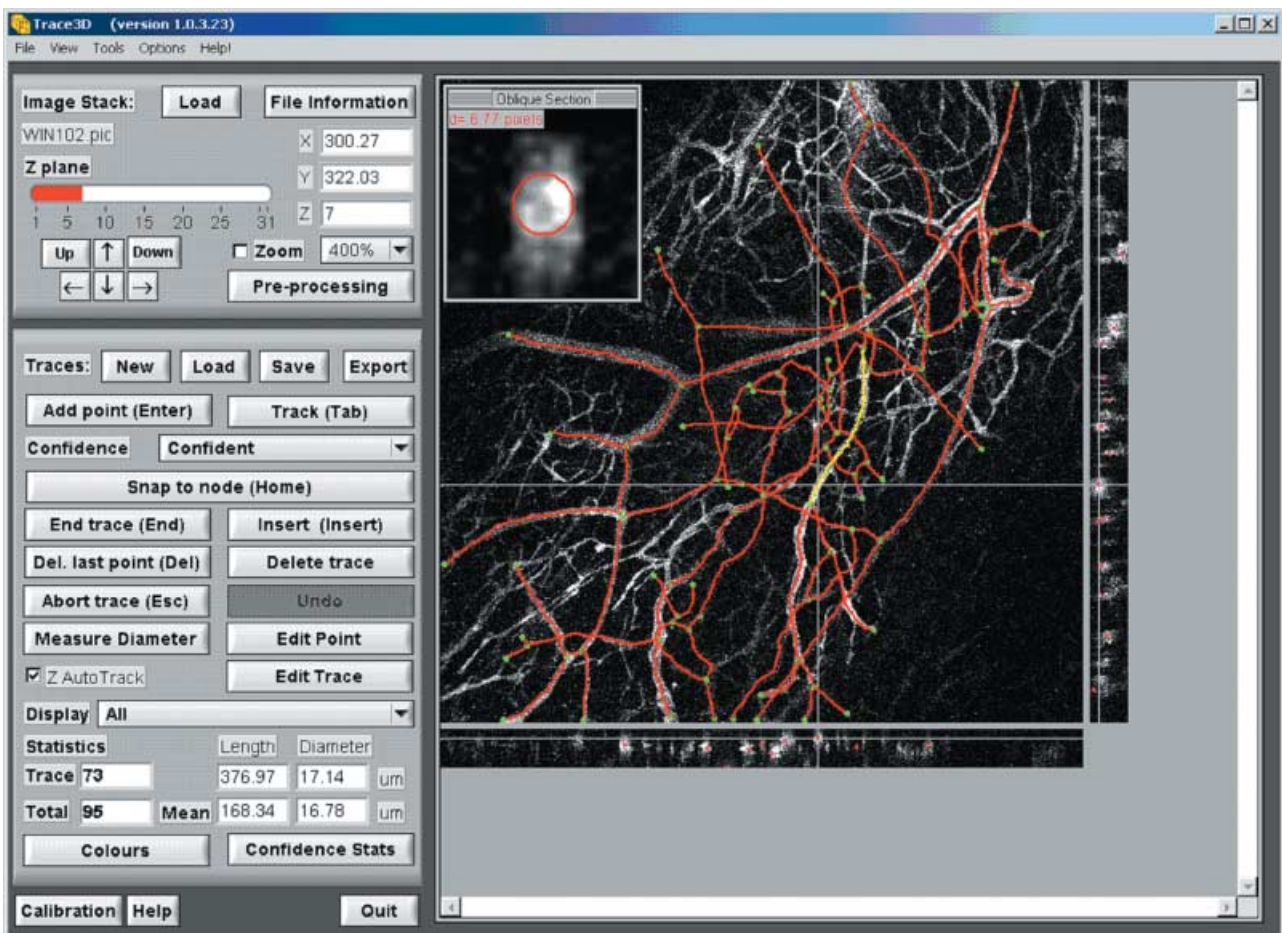


Fig. 1. A screen shot of the tracing software in use. The three-dimensional image being traced is of a vascular tree, *in vivo*, captured with two-photon microscopy.

the specified Z position need only be approximate, which is usual once tracing has started as it is based on the previous trace position, and the system will change the cursor position and XY view accordingly to remain within the Z-plane of the structure (described in the section 'Z-plane auto-tracking').

The general direction of the vessel or linear structure is known from adjacent trace points and this can be used to calculate an oblique cross-section through the structure orthogonal to its direction in 3D space (see 'Image cross-sections'). The use of adjacent points precludes the use of this function for traces with less than two points. The oblique cross-section calculated is used to measure the diameter of the structure at this point using the CHARM algorithm (see 'Diameter measurement'). This also determines a centre of mass for the structure that is used to update the trace point position. When manually tracing, the oblique cross-section is displayed as an image with the measured centre position and diameter overlaid for the user to verify. In the case of incorrect measurement the user can correct it with a single mouse click-and-drag action on the oblique cross-section window.

The automatic measurement of structure centre-position and diameter allows the software to track the remainder of a structure automatically given a start of two manually traced points. Once more than one point is specified and the 'Track' button is pressed, the system will proceed along the structure in a stepwise manner, measuring the diameter and refining the trace position at each point. The size of the steps can be specified on an options panel but steps equal to the current radius are usually successful. The steps and, indeed, the separation of the initial manual points, should not be much greater than the vessel diameter to ensure that the structure is nominally straight between points. A more detailed description of the algorithm is presented below in the section 'Trace storage and export'.

When using difficult-to-track, noisy or unclear data the user can associate one of three confidence levels with each point traced. These have been named 'Confident', 'Tentative' and 'Guesswork' and are displayed in different colours. Using these labels it is easier to quantify the reliability of the data and derive appropriate statistics.

Basic statistics about the tracings are shown on the front panel. Measurement of the trace lengths and mean diameters are made and reported for all traces and the current or selected trace. In addition, several general trace-point deletion, selection and insertion functions have been incorporated for trace editing.

Software and image processing methods

Image cross-sections

Orthogonal cross-sections are created in the XY, XZ or YZ planes by extracting the relevant plane of data from the image stack, and these are only formed at integer values of X, Y and

Z. Zooming is performed by expanding the image for display and interpolating bi-linearly.

Oblique cross-sections are created by calculating the equation of the plane perpendicular to the direction of the linear structure with standard geometry. Values on this plane form the cross-section image and are then calculated from the 3D data set by tri-linear interpolation between the data points. Where appropriate, this image is re-sampled by bi-linear interpolation before display.

Z-Plane auto-tracking

The z-plane auto-track function eases manual location of the structure to be traced, in three dimensions, by automatically locating the nearest bright structure, at the current XY position, by moving the cursor position in the Z direction. Therefore, as the user moves the cursor position in the XY plane, step-wise, along a tubular structure to be traced, the cursor Z position is automatically updated to maintain the cursor position at the centre of the structure.

z-Plane auto-tracking is performed by forming a 1D array of values, which are taken from each Z-plane at the cursor position (x, y). A 'hill-climbing' algorithm is applied to this array to find the nearest peak in intensity. A valley-finding algorithm can be used if the structure is dark compared with the background.

To reduce the effect of noise, the value from each Z-plane used is an average of a square of pixels, typically a 3×3 area. The array formed is further filtered (filtering in the Z-direction) by a three-point moving average.

Diameter measurement

Diameter measurement and centre location of the structure is performed by an algorithm that has been named the compact Hough transform and radial map (CHARM). The compact Hough transform was recently used successfully in an automated colony counter (Barber *et al.*, 2001) and has been reapplied here to find the approximate centre position of circular objects (the shape of most vessels in cross-section). The CHARM algorithm works on an oblique cross-section image centred on an approximate vessel centre. It applies two perpendicular Sobel edge-detection filters (Sobel, 1990). A compact Hough transform is applied to the resulting edge maps and gives the largest response to bright circular objects. The pixel with the greatest response is taken as a point within the structure to be measured. This implementation differs from that previously described only by the fact that floating-point values for the centre location are maintained throughout for improved accuracy.

Radial searching is performed from this centre point to find likely object boundary points (Mouroutis *et al.*, 1998; Barber *et al.*, 2000) based on the response of the Sobel filters. The searching range is based on an approximate seed radius and is

typically 0.75–1.5 times this value. The edges, identified by a significant Sobel response of the correct orientation, form a radial map that describes the shape. Some filtering of this map is required to eliminate distraction from unwanted structure, and the effect of a non-spherical imaging PSF. The 32-point maps were spatially filtered with a three-point median filter. The centre of mass (Russ, 1999) of the 2D shape described by the radial map was taken as an accurate measurement of the vessel centre. The diameter measurement was calculated statistically from the median of the 32 radius measurements.

Linear structure tracking

Linear structure tracking is based on the algorithm for diameter measurement as this also calculates the centre of mass of the structure. The user must provide two points at the start of the structure to seed tracking and the algorithm steps along the structure by estimating the next centre point and updating it whilst measuring the diameter.

The estimate for the next centre position is based on the current direction of the linear structure based on the previous two points. It is assumed that this direction is continued and we move in that direction by a step amount based on the last measured diameter (typically 0.5 times this value). A further enhancement is to take account of the current structure curvature based on the last three points and assume that this continues to the new position.

At the new position, the diameter measurement algorithm is used to measure the structure diameter and to update the centre position. It can sometimes be assumed that the measurement of centre position is much closer to the real position than the estimate, if the data are very clean. More robust tracking, through noisy data, is often achieved by applying a Kalman filter (Maybeck, 1979) to the update of position and diameter measurement. In this case the estimate of the next centre position is formed from a linear combination of the predicted position based on past data and of the measured position based on new data. Ideally, each contribution is inversely weighted by its error but, since these error values are difficult to measure, they are estimated and suitable weights can be arrived at empirically. The filter has been made adaptive by adjusting the weight applied to the new measurement according to the standard deviation of the 32 radial measurements (see 'Diameter measurement'). In this way a higher preference can be given to the new measurement in areas of the data set that are particularly clean and where reliable measurements can be made.

Trace storage and export

Traces are stored in memory in the form of a list of 3D floating-point coordinates, in pixel dimensions. Each point also has a floating-point radius, in pixel dimensions, and a confidence flag associated with it. A trace then consists of an array of

points together with an average diameter and a total length, both in real coordinates. The calibration factors, for conversion to real coordinates, are set by the user via an options panel. The traces can be saved in a text file (*.TRA) as a list of coordinate points, which can be re-loaded into memory.

The traces can also be exported in the form of a virtual reality world file (*.WRL) using the Virtual Reality Modelling Language (VRML) version 2.0, also known as VRML97 (ISO/IEC 14772-1: 1997). The traces can be formed by single pixel lines using the 'IndexedLineSet' geometry or as solid cylinders ('Cylinder' geometry) representing the measured structure diameter. Such files can be imported into 3D rendering packages such as Imaris/Surpass (Bitplane, Zürich, Switzerland) for viewing and for overlaying onto a 3D volume rendering of the original data. In this way the traces can be verified by eye in great detail with the use of 3D zooming, panning and rotation tools.

Development and operational environment

The software was developed under the LabWindows/CVI (National Instruments Corp. Ltd, Newbury, UK) environment in the C programming language and tested on both real and synthetic 3D data sets. The 32-bit application runs on a PC under the Windows NT4, 2000 or XP operating systems. At the Gray Cancer Institute (GCI) the software is run under Windows 2000 (Microsoft, Seattle, WA, U.S.A.) on a PC (Dell, U.K.) with dual Xeon processors (1.7 GHz) (Intel, U.S.A.), 1 Gb of RAM and an Nvidia QuadroPro graphics card (Nvidia, U.S.A.). This computer also runs more computationally intensive visualization software and is more than sufficient to run the tracing software, which has been run comfortably on a single-processor 500-MHz PIII (Intel) PC (Gateway, U.K.) with 128 Mb of RAM using a data-set comprising $512 \times 512 \times 62$ volume elements.

Test methods

The software was primarily developed for the delineation of vascular trees from 3D image data-sets captured with a two-photon microscope. These images are captured *in vivo* via an animal window-chamber arrangement in the dorsal skin flap of a rodent (Tozer *et al.*, 2001). The images were captured with two-photon microscopy at the GCI. The microscope is based on a Nikon TE300 inverted microscope (Nikon UK Ltd, Kingston Upon Thames, U.K.), a Biorad MRC1024MP scanning and detection head (Bio-Rad Laboratories Inc., CA, U.S.A.) and Tsunami femtosecond laser source (Spectra Physics, CA, U.S.A.). Details of this system have been presented in Ameerbeg *et al.* (2002). The intravenous injection of cascade-blue-labelled dextran (30 mg kg^{-1}) provides imaging contrast because it acts as a fluorescent marker of the blood plasma under two-photon excitation at 800 nm.

As a result of the mechanical constraints of the window-chamber model and the need to observe the vasculature of a

large, representative, volume of the tumour, a long-working-distance, low-NA, objective was employed (NIKON CFI 10× Fluor, NA 0.3). The fluorophore was excited at ~800 nm with a laser power of ~25 mW. Measurement of the optical PSF within the sample was estimated with the use of 3- μm fluorescent beads injected via the tail vein of the rodent. A proportion of the beads became trapped within the vascular tree. The observed bead profiles did not differ significantly from those observed in the ideal conditions of slide-mounted beads or the theoretical prediction based on the use of this objective lens. The PSF was approximately 1 μm FWHM in the transverse directions X and Y, and approximately 10 μm in the axial direction, Z.

Testing of the measurement accuracy of the CHARM algorithm was performed on artificial test images. These were created from a binary-image approximation to a circle with a diameter of 10 pixels, which was smoothed and had noise added (see Fig. 2). Resulting images were stacked together to form a 3D image, 20 images deep, which can be traced to produce 18 measurements of centre location and diameter (excluding two measurements at the image extremes). Smoothing was performed by 2D convolution with a floating-point Gaussian kernel with standard deviation (σ) ranging from 0.0 to 5.0 pixels. The kernel size was always four times the standard deviation. Random Gaussian noise with standard deviation (σ) ranging from 0.0 to 50.0 grey levels was added on a pixel-by-pixel basis after smoothing. When forming 3D image stacks from noisy data, noise was added to

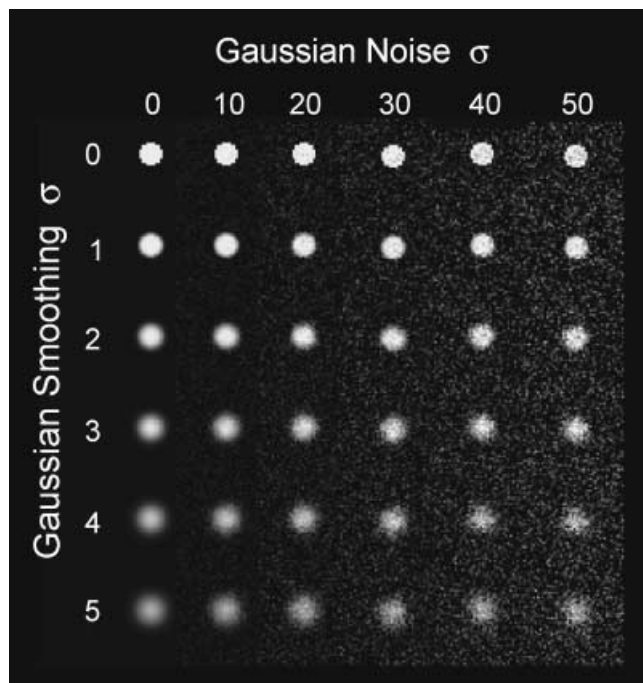


Fig. 2. The basis for the test images was a binary approximation to a circle, to which Gaussian smoothing and noise was added.

each image slice independently. The range of smoothing and degrees of noise were chosen to span those typically observed in real data. The 18 measurements of location and diameter were averaged to ascertain the performance of the algorithm.

The effect of a non-symmetrical imaging PSF on the performance of the algorithm was also demonstrated by applying a 1D Gaussian filter to apply additional smoothing in one direction (see Fig. 6f–j). It is also interesting to demonstrate the ability of the semi-automatic tracing in the presence of a high degree of image smoothing and noise. Three-dimensional images of two, closely spaced, tubular structures were created, based on the binary circle of 10-pixel diameter. In these test images, one tubular structure lies on an arc of radius 50 pixels and is separated at the closest point by one pixel from the second structure, which lies on a straight line (Fig. 7).

Results and discussion

Figure 1 shows a screen shot of the tracing software in use and the XY, XZ and YZ cross-section images can be seen on the right-hand panel overlaid by the lines of tracings already made. The software is in routine use at our institute for the recording and comparison of vascular trees *in vivo*. The results of exporting the traces in VRML format can be seen in Fig. 3. This shows the output of the Imaris visualization software package when loaded with the raw data from the two-photon microscope and the exported VRML-format data from this software. The top-left panel shows a 3D rendering of the raw data using maximum intensity projection. The panel at the top-right shows the virtual reality rendering of a selection of traced vessels greater than 10 μm in diameter (the larger vessels have been traced for clarity). The bottom two panels of Fig. 3 show our ability to trace smaller vessels and capillaries down to ~5 μm in diameter in an expanded maximum-intensity projection (bottom-left panel) and its traced and re-rendered version (bottom-right panel). In this rendering each vessel segment is represented by a cylinder of constant diameter that reflects the mean diameter of the real vessel. Each segment has been capped with a sphere, of the same diameter, on each end to improve the appearance.

The effects of image smoothing and noise on the performance of the algorithm can be seen in Fig. 4. The artificial test images were used to determine an error in the diameter measurement and also in the measured centre location. As expected, the addition of smoothing and noise has a detrimental effect on the measured diameter and centre location. We consider a reasonable extreme smoothing to be 5.0 pixels in width. Below this limit the error in diameter measurement was never above 13% (1.3 pixels in 10.0) and in centre location it was never above 0.7 pixels. It appeared that smoothing is more detrimental than the addition of noise, and additional points, demonstrating how the algorithm begins to fail, are shown in Fig. 4 for smoothing with σ of up to 10.0 pixels in width. The effect of the seed values of approximate vessel

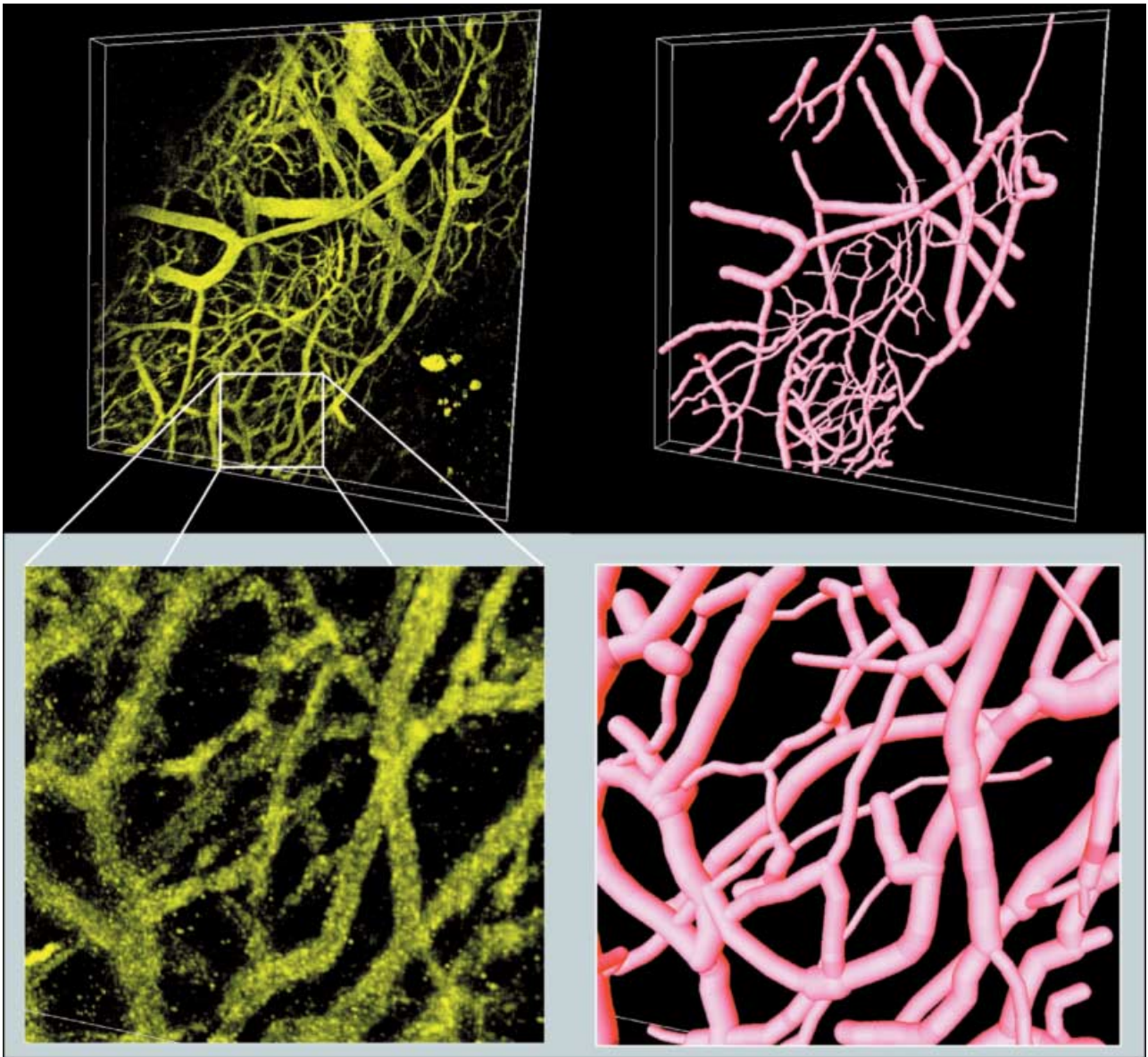


Fig. 3. A three-dimensional rendering of the raw data by maximum intensity projection (top-left panel) and a virtual reality recreation of a traced selection of the larger vessels, for clarity, shown at the same orientation (top-right panel). A small region of the raw data has been expanded in the bottom-left panel. The vessels and capillaries from this region have been traced in greater detail and are shown in the bottom-right panel. All renderings were produced by the Imaris software package (Bitplane, Zürich, Switzerland).

centre and radius were also investigated as functions of smoothing, and the results are presented in Fig. 5. It can be seen that varying the seed centre location has no effect on the measured centre location. However, in practice, the oblique cross-section image, from which the measurement is made, is of finite size and the vessel must be wholly contained within it for the algorithm to succeed. The seed radius must be close enough to the true value for it to be found within the limits of the radial search (typically 0.75–1.5 times the seed value, see 'Diameter measurement') and outside these limits the algorithm fails. Within these limits the error in diameter measurement was

always below 9% (0.9 pixels in 10.0) and the centre was located to within 0.5 pixels. In practice automatic diameter measurement can be seeded by previous measurements at other points on the same vessel whilst tracking or, where no such measurements exist, on an initial manual measurement.

Figure 6 presents a visual indication of the algorithm performance in the presence of symmetrical and non-symmetrical Gaussian smoothing. The diameters measured for symmetrical smoothing of $\sigma = 0.0, 2.0, 4.0, 6.0$ and 8.0 pixels (Fig. 6a–e) were 9.92, 9.92, 9.64, 9.96 and 10.76, respectively (actual diameter 10.0). The addition of 1D smoothing simulates a

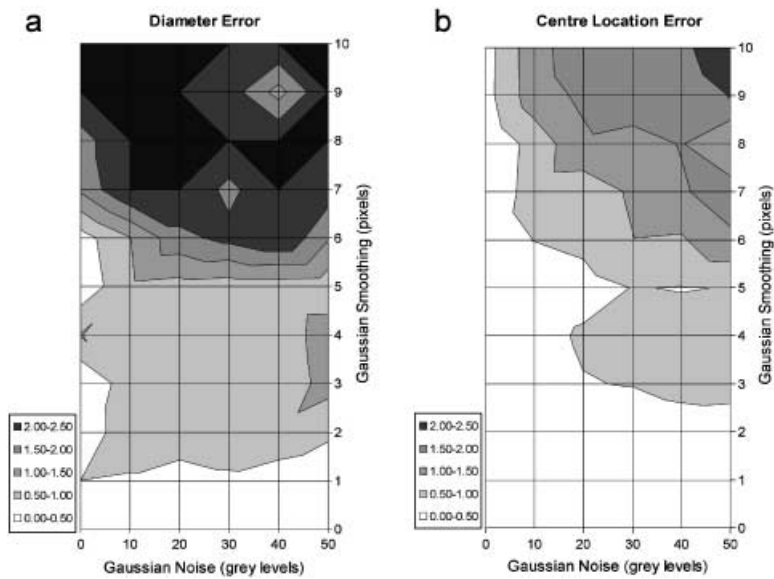


Fig. 4. The error in the measurements of diameter (a) and centre location (b) as a function of image smoothing and noise.

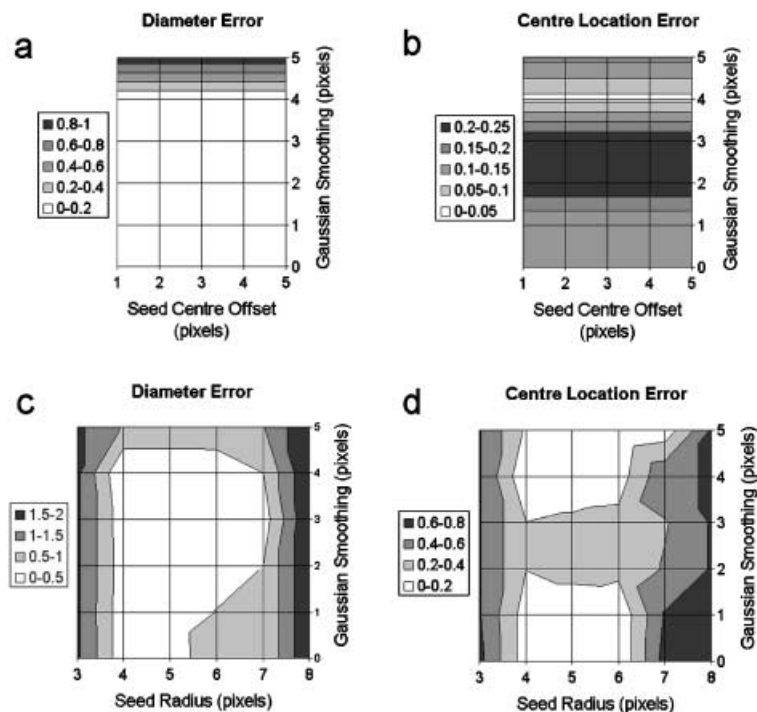


Fig. 5. The error in the measurements of diameter (a,c) and centre location (b,d) as a function of image smoothing and an offset in the seed centre pixel (a,b) or varying seed radius (c,d) used to initialize the CHARM algorithm.

non-symmetrical PSF. Symmetrical smoothing of width 1.0 was augmented by directional smoothing of $\sigma = 2.0, 4.0, 6.0, 8.0$ and 10.0 pixels (Fig. 6f–j). The measured diameters were 9.93, 9.98, 10.05, 10.14 and 10.51, respectively.

Three examples of tracing closely spaced tubular structures are presented in Fig. 7. Subimages a, b and c show cross-sections through the image stacks. No smoothing or noise was added to the image shown in a, whereas b and c were smoothed with σ of 5.0 and 6.0 pixels, respectively, and both had noise of $\sigma = 50.0$ pixels added. Subimages d, e and f show

qualitatively the results of automatic tracing that has been seeded by two points represented by the arrows in Fig. 7(d). Figure 7(e) shows the successful segmentation of the two structures whereas Fig. 7(f) shows how the algorithm may fail by merging the two structures.

Conclusions

We have presented a software application that enables the user to delineate and trace linear structures in three dimensions

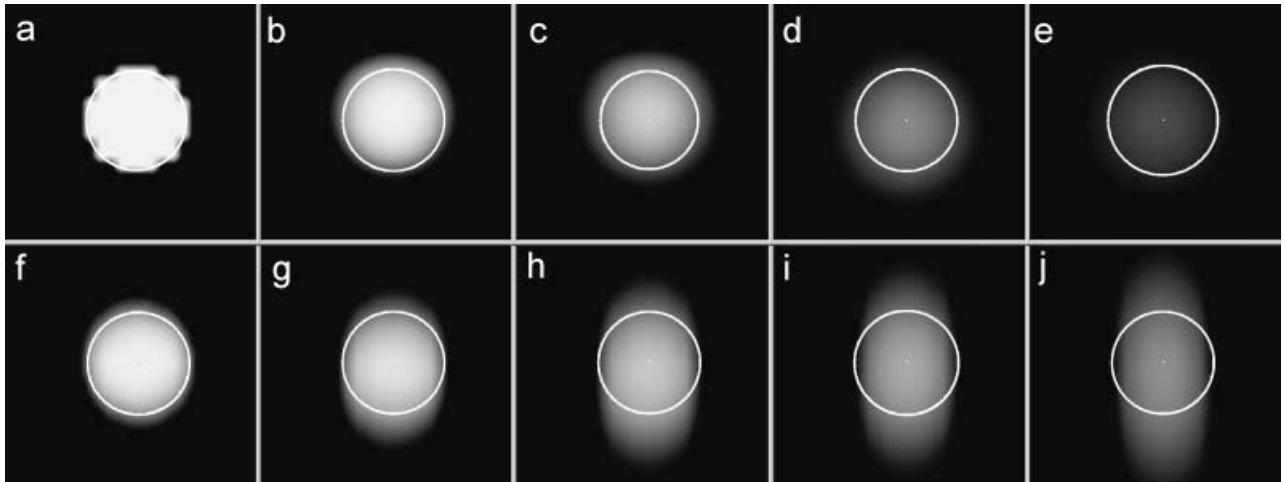


Fig. 6. Results of diameter measurement of a circle with true diameter of 10.0 pixels (a), with symmetrical Gaussian smoothing of $\sigma = 2.0, 4.0, 6.0$ and 8.0 pixels (b, c, d and e, respectively), and with 1D smoothing of $\sigma = 2.0, 4.0, 6.0, 8.0$ and 10.0 pixels (in addition to symmetrical smoothing of $\sigma = 1.0$) (f, g, h, i and j, respectively).

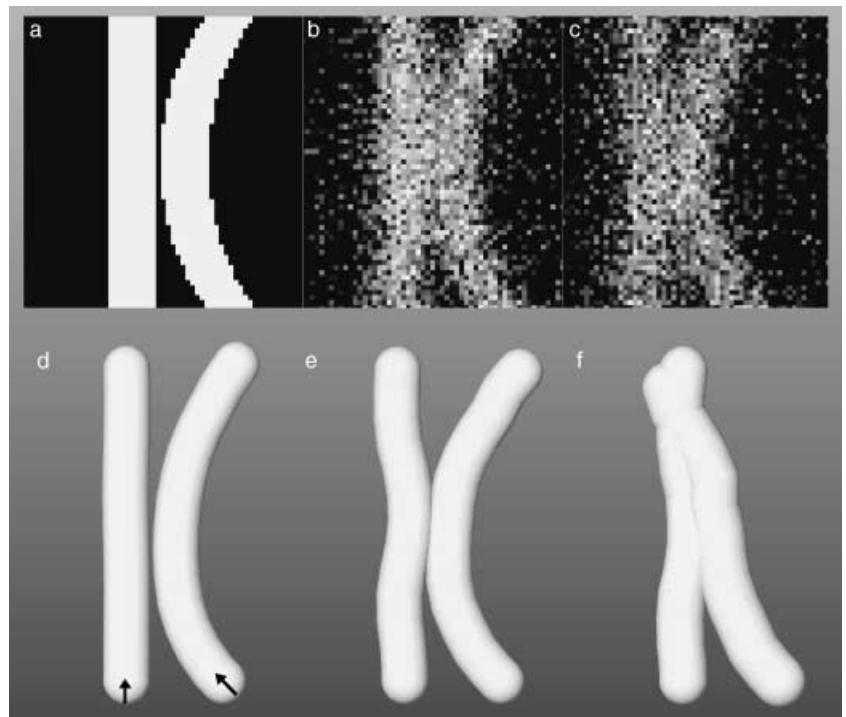


Fig. 7. Tracing two tubular structures that are separated by one pixel at the closest point. Shown are cross-sections through the centre of the volume data with no noise or smoothing (a) and with Gaussian noise added ($\sigma = 50.0$) and smoothing of $\sigma = 5.0$ (b) and 6.0 (c). The results of automatic tracing are represented in d to f, the arrows in d indicating the given starting points for tracing.

semi-automatically. The software was written to collect data on vascular networks *in vivo* within the animal window-chamber model. This has been achieved by employing two-photon microscopy and the software presented. However, the software package is equally applicable to similar problems involving 3D volumetric data sets from other sources, such as the tracing of neurons or bone structures.

Storage of the traced structures in a text file exports all the information necessary to recreate the structure in other software packages. This will allow additional data analysis packages

to be written that quantify statistics about the structure. For example, the mean distance between vessels branches, the mean diameter and branching angle are all of interest when quantifying the differences in vascular structure between normal and tumour tissue. Other more complex measures such as fractal dimension, which may prove useful for the same purpose, can also now be made.

Export of the structure in virtual reality (VRML) format allows the easy validation of the traced structures by eye using commercially available rendering packages in the fully 3D

arena. It could be argued that it would be ideal to trace and visualize in three dimensions using fully integrated virtual-reality immersion hardware but this solution is both financially and computationally expensive. In any case, tracing large vascular trees is particularly labour-intensive and requires a high degree of concentration from the operator who may suffer from fatigue. The use of a simpler software-only solution allows the operator to perform tracing in a comfortable environment, at the computer of choice, which would not be the case with a custom-built virtual-reality solution.

Through the use of the Hough transform the algorithm is capable of detecting multiple vessel centres, if they exist, within the oblique cross-section. In this way it should be possible to detect and locate branching points, in three dimensions, by the change to a bimodal distribution, in a way similar to the 2D algorithm of Tolias & Panas (1998).

Acknowledgements

We would like to thank to Dr V. E. Prise for help and expertise in preparation of the window chambers. We also gratefully acknowledge the support of Cancer Research UK under programme grant C133/A1812 – SP2195-01/02.

References

- Ameer-Beg, S.M., Barber, P.R., Hodgkiss, R.J., Locke, R.J., Newman, R.G., Tozer, G.M., Vojnovic, B. & Wilson, J. (2002) Application of multiphoton steady state and lifetime imaging to mapping of tumour vascular architecture in vivo. *Proc. SPIE*, **4620**, 85–95.
- Barber, P.R., Vojnovic, B., Kelly, J., Mayes, C.R., Boulton, P., Woodcock, M. & Joiner, M.C. (2000) An automated colony counter utilising a compact Hough transform. *Proceedings of Medical Image Understanding and Analysis, MIUA2000*, (ed. by S. Arridge and A. Todd-Pokropek), pp. 41–44, UCL, London.
- Barber, P.R., Vojnovic, B., Kelly, J., Mayes, C.R., Boulton, P., Woodcock, M. & Joiner, M.C. (2001) Automated counting of mammalian cell colonies. *Phys. Med. Biol.* **46**, 63–76.
- Brown, E.B., Campbell, R.B., Tsuzuki, Y., Xu, L., Carmeliet, P., Fukumura, D. & Jain, R.K. (2001) *In vivo* measurement of gene expression, angiogenesis and physiological function in tumors using multiphoton laser scanning microscopy. *Nature Med.* **7**, 864–868.
- Bulpitt, A.J. & Berry, E. (1998) An automatic 3D deformable model for segmentation of branching structures compared with interactive region growing. *MIUA*, **98** (ed. by S.E. Berry, D.C. Hogg, K.V. Mardia and M.A. Smith), pp. 25–28, University Print Services, Leeds.
- Maybeck, P.S. (1979) *Stochastic Models, Estimation, and Control*. Academic Press Inc., New York.
- Mouroutis, T., Roberts, S.J. & Bharath, A.A. (1998) Robust cell nuclei segmentation using statistical modelling. *Bioimaging*, **6**, 79–91.
- Russ, J.C. (1999) *The Image Processing Handbook*. CRC Press, New York.
- Serra, L., Hern, N., Choon, C.B. & Poston, T. (1997) Interactive vessel tracing in Volume data. *ACM Symposium on Interactive 3D Graphics* (ed. by M. Cohen and D. Zeltzer), pp. 131–137, ACM Press, New York.
- Sobel, I. (1990) An isotropic 3×3 image gradient operator. *Machine Vision for Three-Dimensional Scenes* (ed. by H. Freeman), pp. 376–379, Academic Press, New York.
- Tolias, Y.A. & Panas, S.M. (1998) A fuzzy vessel tracking algorithm for retinal images based on fuzzy clustering. *IEEE Trans. Med. Imaging*, **17**, 263–273.
- Tozer, G.M., Prise, V.E., Wilson, J., Cemazar, M., Shan, S., Dewhurst, M.W., Barber, P.R., Vojnovic, B. & Chaplin, D.J. (2001) Mechanisms associated with tumor vascular shut-down induced by combretastatin A-4 phosphate: intravital microscopy and measurement of vascular permeability. *Cancer Res.* **61**, 6413–6422.